Dalton Transactions

Accepted Manuscript

ROYAL SOCIETY OF CHEMISTRY

www.rsc.org/dalton

Multiple magnetic relaxation processes, magnetocaloric effect and fluorescent properties of rhombus-shaped tetranuclear rare earth complexes

Hong-Ling Gao, Li Jiang, Shuang Liu, Hai-Yun Shen, Wen-Min Wang and Jian-Zhong Cui*[1]

ABSTRACT: Seven new tetranuclear rare earth (RE) complexes [$RE_4(acac)_4L_6(\mu_3\text{-}OH)_2$] (HL = 5-(4-fluorobenzylidene)-8-hydroxylquinoline; acac = acetylacetonate; RE = Y (**1**), Eu (**2**), Gd (**3**), Tb (**4**), Dy (**5**), Tm (**6**) and Lu (**7**)) have been synthesized and completely characterized. Complex **5** exhibits multiple zero-field slow magnetic relaxation processes typical for Single Molecular Magnets (SMMs). Two distinct slow magnetic relaxation processes, with effective energy barriers U_{eff} = 48 K for slow relaxation (SR) process and U_{eff} = 121 K for fast relaxation (FR) process, are mainly attributed to the presence of two crystallographically independent Dy(III) sites. The magnetocaloric effect (MCE) was detected with $-\Delta S_m(T)$ = 20.8 J kg^{-1} K^{-1} for complex **3**. The fluorescent properties of complexes **1**, **2**, **4**, **5**, **7** were also investigated. Complexes **2**, **4**, **5** show their characteristic peaks for the corresponding RE(III) center, while complexes **1** and **7** show the similar emission peaks with the Schiff base ligand when they were excited at the appropriate wavelength.

[1]Department of Chemistry, Tianjin University, Tianjin 300072, People's Republic of China

Corresponding author. *E-mail:* cuijianzhong@tju.edu.cn (J.-Z. Cui).

†Electronic supplementary information (ESI) available: ^{1}H NMR spectrum, PXRD patterns, TGA, additional magnetic measurements, selected bond lengths and angles, the fitting parameters from cole-cole plots.

INTRODUCTION

Rare earth complexes have been experiencing a period of vigorous development in recent years.[1] The reason for the interest in such complexes is driven not only from a strictly fundamental aspect, but also by potential technological applications in various areas such as sensors,[2] information storage,[3] spintronics,[4] quantum computing.[5] For the research field of molecular magnetism, single molecular magnets (SMMs) with high effective barriers (U_{eff}) and blocking temperatures (T_B), magnetocaloric effects，or magneto-structural correlations are always the focus of concentrations for researchers.[6] Especially, since the first SMM of archetypal $[Mn_{12}O_{12}(OCR)_{16}(H_2O)_4]$ was reported in 1993, SMM complexes of varying configurations have been experiencing a rapid expansion.[7] The anisotropic barrier (U) of a SMM is derived from a combination of an appreciable spin ground state (S) and uniaxial Ising-like magneto-anisotropy (D).[8] For the lanthanide system, the significant single-ion magnetic anisotropy arising from the large unquenched orbital angular momentum and strong spin–orbit coupling is the key in determining the magnetization reversal barrier and the T_B.[9] So far, a number of pure lanthanide-based SMMs have been described in the literatures.[10] Most of them contain Dy(III) or Tb(III) ions within different network topologies, derived from mononuclear, dimeric, triangular, defect-dicubane, square-pyramidal core or a trigonal bipyramidal.[10e-j] Among them, the studies of tetranuclear Dy-SMMs, particularly of multi-relaxations Dy_4 SMMs with different structural types have played important roles in exploring high energy barrier SMM properties and understanding the magnetic relaxation pathway.[7l, 11] For example, a defect-dicubane Dy_4 SMM with an anisotropic barrier of 170 K[11a] and a linear Dy_4 SMM with an anisotropic barrier of 173K have been reported to show two separate relaxation processes and provide an abundant platform for us to study the magneto-structural correlations of Ln-SMMs. [11b] A latest square grid dual-relaxations Dy_4 SMM $[Dy_4(OH)_2(bpt)_4(NO_3)_4(OAc)_2]$ with the highest energy barrier (206K) among the pure Dy_4 SMMs under zero direct current (dc) field was reported by Tong et al..[11f]

Recently, a number of Schiff base and β-diketonate ligands have been successfully used in the construction of magnetic and fluorescent materials.[4b,7e,12] As we all know, 8-hydroxyquinoline and its derivatives are known as a class of highly fluorescent materials as well as promising materials for nonlinear optical properties and electroluminescent applications.[13] β-diketonates are not only ideal candidates as light-harvesting chromospheres,[14] but also suited to the investigation

in the field of SMMs.[15] Based on the comprehensive consideration of magnetic and fluorescent properties, we have designed and synthesized a 8-hydroxyquinolone-based Schiff base ligand. It was formed by the condensation of 5-amino-8-hydroxyquinoline and 4-fluorobenzaldehyde. The targeted ligand (HL) has a large conjugated system leading to a relatively rigid structure and the versatile oxygen and nitrogen coordination modes. Herein, we report a series of rhombus-shaped tetranuclear rare earth complexes $[RE_4(acac)_4L_6(\mu_3\text{-}OH)_2]$ (RE = Y (**1**), Eu (**2**), Gd (**3**), Tb (**4**), Dy (**5**), Tm (**6**) and Lu (**7**)). Among them, complexes **1**, **2**, **4**, **5**, **7** show their typical fluorescent properties. The magnetocaloric effect (MCE) was detected with $-\Delta S_m(T)$ = 20.8 J kg^{-1} K^{-1} for complex **3**. Strikingly, complex **5** exhibits multiple zero-field slow magnetic relaxation processes typical for SMMs. As far as we know it is another multi-relaxations Dy_4 SMM with relatively high energy barrier (121K) under zero dc field.

EXPERIMENTAL SECTION

Materials and Measurements. Manipulations of all complexes were performed in air atmosphere. $RE(acac)_3{\cdot}2H_2O$ (RE = Y, Eu, Gd, Tb, Dy, Tm and Lu) were prepared according to the literature procedure previously described.[16] 5-(4-fluorobenzylidene)-8-hydroxylquinoline (HL) was prepared from the reaction of 5-amino-8-hydroxylquinoline and 4-fluorobenzaldehyde (Scheme 1). Other chemicals were commercially available and generally used without further purification. Infrared spectra were recorded on a Bruker TENOR27 spectrophotometer in the range of 4000–400 cm^{-1} (KBr pellets). UV-vis spectra were recorded with a TU-1901 UV-Vis spectrometer (Shanghai, China). The ^1H NMR spectrum was tested on a Bruker AVANCE Ⅲ NMR spectrometer. The C, H, N microanalyses were carried out with a PerkinElmer 240 CHN elemental analyzer. Powder X-ray diffraction (PXRD) data were performed on a Rigaka D/max 2500 v/pc X-ray powder diffractometer with Cu-Kα radiation (λ = 1.540598 Å). Thermogravimetric analyses (TGA) were prepared on a NETSCH 409 PC instrument with a heating rate of 10 ºC min^{-1}. Fluorescence spectra were measured with a Cary Eclipse luminescence spectrophotometer at room temperature. Variable temperature (2–300 K) dc magnetic susceptibility, alternating current (ac) susceptibility measurements and variable field (0–8 T) magnetization measurements were carried out on a SQUID PPMS ACMS magnetometer. Diamagnetic corrections were made with Pascal's constants for all of the constituent atoms.[17] All crystalline samples characterized by PXRD, TG, EA, IR, UV-Vis, fluorescent and magnetic

studies were pre-treated by keeping the obtained samples for a period of time at ambient conditions leading to the disordered solvent molecules losing spontaneously. The crystalline samples used for all measurements were obtained from the same batch.

Synthesis of 5-(4-fluorobenzylidene)-8-hydroxylquinoline.

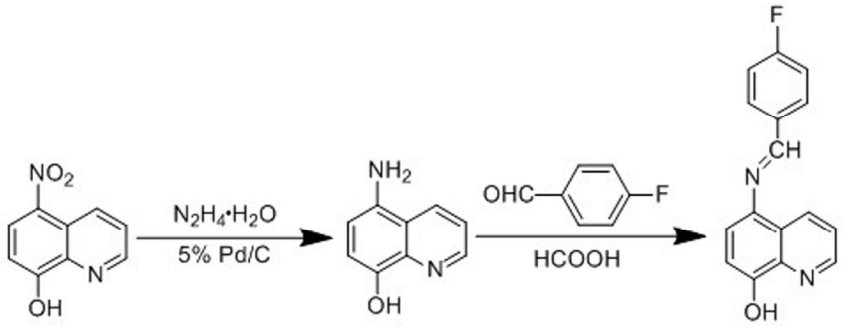

Scheme 1. The synthesis route of 5-(4-fluorobenzylidene)-8-hydroxylquinoline.

5-amino-8-hydroxylquinoline. The synthesis of 5-amino-8-hydroxyquinoline is optimized compared to the method from the previously reported literature.[18] The mixture of 5-nitryl-8-hydroxylquinoline (4.75 g, 0.025 mol) and 5% Pd/C (0.0625 g) used as catalyst in a 1.3% ratio in absolute isopropanol was heated to 70 ℃, and then 5 mL 80% hydrazine hydrate was dropped into the mixture in 30 minutes. It was heated to reflux at 92 ºC for 4 h. Finally, the solvent was removed, and then dichloromethane was used to wash the grass green solid product (yield 2.7 g, 67.5%). Elemental analysis (%): Calcd. for $C_9H_8ON_2$ (fw = 160.42): C, 67.50; H, 5.00; N, 17.50; Found: C, 67.28; H, 4.73; N, 17.82. IR (cm^{-1}): 3344 (s), 1688 (s), 1626 (s), 1489 (s), 1346 (s,), 915 (s), 746(m).

5-(4-fluorobenzylidene)-8-hydroxylquinoline. 5-amino-8-hydroxylquinoline (0.8 g, 5 mmol) was dissolved in 30 mL of ethanol at 60 ℃, 1.5 mL 4-fluorobenzaldehyde was added, and 3−4 drops of formic acid were dropped as catalyst. After that the mixture was heated for 4 h at 83 ℃. The product was isolated from the mixture and it was purified by recrystallization from the mixed solvent of ethanol and acetone (3/1, V/V). The purified product was obtained as a green solid (yield 1.12 g, 84.2%). Elemental analysis (%): Calcd. for $C_{16}H_{11}FON_2$ (fw = 266.20): C, 72.17; H, 4.14; N, 10.52. Found: C, 71.86; H, 3.92; N, 10.22. IR (cm^{-1}): 3060(w), 2859(w), 1591(m), 1508(vs), 1467(m), 1411(s), 1286(s), 1245(s), 1197(s), 1141(m), 1050(w), 961(w),

822(m), 780(m), 704(w), 614(w), 510(w), 455(w). UV-vis spectrum in CH_3OH [λ_{max} (nm)]: 210, 250, 367. Melting point: 180–182 ℃. ^1H NMR ($CDCl_3$, δ, ppm): 8.62 (s, 1H, N=CH-), 7.20–8.87 (m, Ar-H) (Fig. S1†).

Syntheses of complexes 1–7. RE(acac)$_3$·2H$_2$O (0.03 mmol) (RE = Y (**1**), Eu (**2**), Gd (**3**), Tb (**4**), Dy (**5**), Tm (**6**) and Lu (**7**)) was dissolved in 15 mL acetonitrile. Then 5 mL CH_2Cl_2 solution of HL (0.0080 g, 0.03 mmol) was added to the stirred acetonitrile solution, and the mixture was heated for 2 h at 70 °C. Finally, the solution was cooled to room temperature and filtered. Yellow block crystals suitable for single crystal X-ray diffraction analysis were isolated by keeping the filtrate at 4 °C for three days.

[Y_4(acac)$_4$L$_6$(μ_3-OH)$_2$] (**1**). Yield: 0.030 g, 42.3%. Elemental analysis (dried sample) (%): Calcd. for [Y_4(acac)$_4$L$_6$(μ_3-OH)$_2$]: C, 58.60; H, 3.82; N, 7.07; Found: C, 58.83; H, 3.58; N, 7.39. IR (cm^{-1}): 3635(w), 3060(w), 2859(w), 1598(vs), 1502(s), 1459(s), 1383(s), 1307(s), 1238(m), 1141(w), 1085(m), 1009 (w), 933(w), 836(m), 760(m), 732(w), 608(w), 511(w), 469(w).

[Eu_4(acac)$_4$L$_6$(μ_3-OH)$_2$] (**2**). Yield: 0.028 g, 36.2%. Elemental analysis (dried sample) (%): Calcd. for [Eu_4(acac)$_4$L$_6$(μ_3-OH)$_2$]: C, 52.98; H, 3.45; N, 6.39. Found: C, 52.63; H, 3.33; N, 6.62. IR (cm^{-1}): 3621(w), 2865(w), 1598(vs), 1508(s), 1453(s), 1384(s), 1314(s), 1224(m), 1148(w), 1092(m), 1009(w), 919(w), 836(m), 760(w), 726(w), 649(w), 601(w), 517(w), 476(w).

[Gd_4(acac)$_4$L$_6$(μ_3-OH)$_2$] (**3**). Yield: 0.024 g, 30.5%. Elemental analysis (dried sample) (%): Calcd. for [Gd_4(acac)$_4$L$_6$(μ_3-OH)$_2$]: C, 52.56; H, 3.42; N, 6.34. Found: C, 52.27; H, 3.19; N, 6.63. IR (cm^{-1}): 3621(w), 3073(w), 2859(w), 1591(vs), 1508(s), 1467(s), 1390(s), 1314(s), 1238(m), 1155(w), 1099(m), 1023(w), 919(w), 836(m), 767(w), 718(w), 649(w), 601(w), 510(w), 469(w).

[Tb_4(acac)$_4$L$_6$(μ_3-OH)$_2$] (**4**). Yield: 0.036 g, 45.8%. Elemental analysis (dried sample) (%): Calcd. for [Tb_4(acac)$_4$L$_6$(μ_3-OH)$_2$]: C, 52.42; H, 3.41; N, 6.32. Found: C, 52.19; H, 3.20; N, 6.63. IR (cm^{-1}): 3642(w), 3048(w), 2856(w), 1580(vs), 1500(s), 1462(s), 1376(s), 1308(s), 1216(m), 1136(w), 1068(m), 1005(w), 925(w), 818(m), 760(m), 732(w), 608(w), 510(w), 469(w).

[Dy_4(acac)$_4$L$_6$(μ_3-OH)$_2$] (**5**). Yield: 0.039 g, 48.6%. Elemental analysis (dried sample) (%): Calcd. for [Dy_4(acac)$_4$L$_6$(μ_3-OH)$_2$]: C, 52.14; H, 3.40; N, 6.29. Found: C, 52.28; H, 3.18; N, 6.52.

IR (cm^{-1}): 3621(w), 3067(w), 2866(w), 1598(vs), 1501(s), 1459(s), 1390(s), 1308(s), 1231(m), 1154(w), 1085(m), 1016(w), 919(w), 836(m), 767(w), 711(w), 649(w), 594(w), 525(w), 462(w).

$[Tm_4(acac)_4L_6(\mu_3\text{-}OH)_2]$ (**6**). Yield: 0.028 g, 34.1%. Elemental analysis (dried sample) (%): Calcd. for $[Tm_4(acac)_4L_6(\mu_3\text{-}OH)_2]$: C, 51.65; H, 3.36; N, 6.23. Found: C, 51.42; H, 3.08; N, 6.55. IR (cm^{-1}): 3620(w), 2868(w), 1586(vs), 1502(s), 1436(s), 1370(s), 1316(s), 1224(m), 1148(w), 1088(m), 1009(w), 919(w), 836(m), 766(w), 720(w), 645(w), 601(w), 517(w), 476(w).

$[Lu_4(acac)_4L_6(\mu_3\text{-}OH)_2]$ (**7**). Yield: 0.031 g, 38.4%. Elemental analysis (dried sample) (%): Calcd. for $[Lu_4(acac)_4L_6(\mu_3\text{-}OH)_2]$: C, 51.19; H, 3.33; N, 6.18. Found: C, 51.32; H, 3.06; N, 6.46. IR (cm^{-1}): 3630(w), 3068(w), 2844(w), 1598(vs), 1502(s), 1462(s), 1380(s), 1309(s), 1256(m), 1141(w), 1049(m), 1009(w), 942(w), 836(m), 758(m), 736(w), 608(w), 511(w), 469(w).

X-ray single crystal structure determination. Crystallographic data of **1**−**7** were carried out on a BRUKER SMART-1000 CCD diffractometer with graphite monochromatic Mo Kα radiation (λ = 0.71073 Å) by using ω–$\varnothing$ scan at 113(2) K. The crystals did not degrade during the data collections. The structures were solved by direct method and refined anisotropically by full-matrix least-squares methods based on F^2 with the SHELXL program package for all non-hydrogen atoms.[19] Hydrogen atoms were located and included at their calculated positions. The crystals were measured as soon as isolated from the solution, thus there were some disordered solvent molecules. The free solvent molecules were removed via "SQUEEZE" due to the extreme disorder which could not be solved. The fluorophenyl ring from the Schiff base ligand displays a two-fold orientational disorder with fluorine atoms pointing in opposite sides of the ring, with the occupation of 0.540/0.460 for **1**, 0.629/0.371 for **2**, 0.605/0.395 for **3**, 0.588/0.412 for **4**, 0.562/0.438 for **5**, 0.563/0.437 for **6** and 0.582/0.418 for **7**. Crystallographic data and details of structural determination refinement are summarized in Table 1, and the selected bond lengths and angles have been provided in the Electronic Supplementary Information, Table S1†. CCDC 1401357(**1**), 1401352(**2**), 1401353(**3**), 1434421(**4**), 1404811(**5**), 1401356(**6**) and 1401354(**7**) contain the supplementary crystallographic data for complexes **1**−**7**. These data can be obtained free of charge from the Cambridge Crystallographic Data Centre via www.ccdc.cam.ac.uk/data request/cif.

Table 1. Crystallographic Data and Structure Refinements for complexes **1**−**7.**

Complex	**1**	**2**	**3**	**4**	**5**	**6**	**7**
Formula	$C_{116}H_{90}F_6N_{12}O_{16}Y_4$	$C_{116}H_{90}F_6N_{12}O_{16}Eu_4$	$C_{116}H_{90}F_6N_{12}O_{16}Gd_4$	$C_{116}H_{90}F_6N_{12}O_{16}Tb_4$	$C_{116}H_{90}F_6N_{12}O_{16}Dy_4$	$C_{116}H_{90}F_6N_{12}O_{16}Tm_4$	$C_{116}H_{90}F_6N_{12}O_{16}Lu_4$
Formula weight	2377.63	2629.83	2650.99	2657.67	2671.99	2697.71	2721.87
Crystal system	Orthorhombic	Orthorhombic	Orthorhombic	Orthorhombic	Orthorhombic	Orthorhombic	Orthorhombic
Space group	*Pbcn*	*Pbcn*	*Pbcn*	*Pbcn*	*Pbcn*	*Pbcn*	*Pbcn*
a (Å)	14.330(3)	14.339(3)	14.350(3)	14.2890(7)	14.296(3)	14.271(3)	14.318(3)
b (Å)	26.134(5)	26.055(5)	26.024(5)	26.0134(12)	26.078(5)	26.159(5)	26.201(5)
c (Å)	30.745(6)	31.083(6)	31.000(6)	30.9029(14)	30.889(6)	30.634(6)	30.477(6)
Volume ($Å^3$)	11514(4)	11613(4)	11577(4)	11486.8(9)	11516(4)	11437(4)	11434(4)
Z	4	4	4	4	4	4	4
Calculated density($Mg\ m^{-3}$)	1.372	1.504	1.521	1.537	1.541	1.567	1.581
Abs coeff (mm^{-1})	2.072	2.206	2.338	2.509	2.642	3.150	3.500
F (000)	4832	5216	5232	5248	5264	5312	5344
Crystal size (mm)	0.18 × 0.18 × 0.10	0.20 × 0.18 × 0.10	0.18 × 0.16 × 0.10	0.20 × 0.18 × 0.12	0.22 × 0.20 × 0.12	0.20 × 0.18 × 0.12	0.22 × 0.18 × 0.12
θ range (°)	1.69–25.02	1.31–25.02	1.31–25.02	3.03–27.53	1.75–25.02	1.56–25.02	1.34–25.02
Limiting indices	$-17 \le h \le 14$ $-30 \le k \le 31$ $-36 \le l \le 36$	$-17 \le h \le 17$ $-30 \le k \le 30$ $-36 \le l \le 34$	$-15 \le h \le 17$ $-30 \le k \le 30$ $-36 \le l \le 36$	$-18 \le h \le 18$ $-33 \le k \le 33$ $-40 \le l \le 37$	$-16 \le h \le 16$ $-30 \le k \le 30$ $-36 \le l \le 33$	$-16 \le h \le 16$ $-31 \le k \le 30$ $-36 \le l \le 30$	$-17 \le h \le 17$, $-31 \le k \le 31$, $-36 \le l \le 336$
Reflections collected	81183	82007	82358	138506	79473	55095	84212
Independent reflection	10163 [*R*(int) = 0.0746]	10242 [*R*(int) = 0.0991]	10208 [*R*(int) = 0.1011]	13192 [*R*(int) = 0.0396]	10128 [*R*(int) = 0.0761]	10065 [*R*(int) = 0.0499]	10090 [*R*(int) = 0.0549]
Completeness	99.9%	100.0 %	100.0 %	99.6 %	99.8 %	99.8 %	100.0 %
Max. and min. transmission	0.8196 and 0.7067	0.8095 and 0.6667	0.7999 and 0.6783	0.7528 and 0.6338	0.7422 and 0.5941	0.7037 and 0.5715	0.6788 and 0.513
Data / restraints / parameters	10163 / 96 / 746	10242 / 96 / 746	10208 / 96 / 746	13192 / 100 / 771	10128 / 96 / 746	10065 / 96 / 746	10090 / 96 / 746
GoF on F^2	1.111	1.137	1.137	1.106	1.099	1.167	1.217
Final *R* indices [$I>2\sigma(I)$]	$R_1{}^a = 0.0600$ $wR_2{}^b = 0.1356$	$R_1{}^a = 0.0643$ $wR_2{}^b = 0.1522$	$R_1{}^a = 0.0666$ $wR_2{}^b = 0.1626$	$R_1{}^a = 0.0286$ $wR_2{}^b = 0.0580$	$R_1{}^a = 0.0438$ $wR_2{}^b = 0.0920$	$R_1{}^a = 0.0402$ $wR_2{}^b = 0.1037$	$R_1{}^a = 0.0477$ $wR_2{}^b = 0.1287$
R indices (all data)	$R_1 = 0.0771$ $wR_2 = 0.1461$	$R_1 = 0.0854$ $wR_2 = 0.1658$	$R_1 = 0.0888$ $wR_2 = 0.1793$	$R_1 = 0.0360$ $wR_2 = 0.0605$	$R_1 = 0.0524$ $wR_2 = 0.0963$	$R_1 = 0.0459$ $wR_2 = 0.1071$	$R_1 = 0.0524$ $wR2 = 0.1323$
Largest diff. peak and hole($e\ Å^{-3}$)	0.797 and -0.763	1.194 and -1.318	1.423 and -1.322	1.188 and -0.568	1.106 and -0.936	0.841 and -1.544	1.065 and -1.857

[a] ${}^aR_1 = \Sigma(||F_o|-|F_c||)/\Sigma|F_o|$; [b] ${}^bwR_2 = [\Sigma w(|F_o|^2-|F_c|^2)^2/\Sigma w(F_o^2)^2]^{1/2}$.

RESULTS AND DISCUSSION

Descriptions of the complexes. Single-crystal X-ray diffraction studies reveal that all complexes **1**−**7** crystallize in the orthorhombic *Pbcn* space group. They are isomorphic and complex **5** is selected as a representative example to describe the structure in detail. The core structure of **5** has a tetranuclear arrangement of Dy(III) ions with crystallographic inversion symmetry (Fig. 1). In the centrosymmetric unit, the Dy1 and Dy2 ions are eight coordinated, and their coordination polyhedrons can be described as a distorted square-antiprismatic geometry (Fig. 2). The Dy1 ion is coordinated to seven oxygen atoms and one nitrogen atom, while six oxygen atoms and two nitrogen atoms form the coordination sphere around Dy2 ion. The two square bases of the square antiprism for Dy1 consist of O1, O8a, O8, N1 and O2a, O3a, O4, O5, whereas for Dy2, the two square bases are defined by the atoms O1, O8a, O6, O7 and N3, N5, O2, O3. A square antiprism can be described by an angle (α) describing its elongation or flatness.[20] For a soft-sphere model with a repulsion energy law $\alpha \approx 1/r^6$, the ideal α value amounts to 57.16º. For Dy1 ion in **5**, the hemisphere including the atoms O1, O8, O8a, and N1 is strongly distorted since the angles α of 52.10(1)º and 57.52(1)º are deviated from the theoretical values by 5.06 and 0.81º for a square antiprism. This distortion is most likely due to the small bite angle of μ_3-OH ligands (O8–Dy1–O8a = 71.82(3)º). The second hemisphere with α of 57.92(6)º and 59.48(5)º close to the ideal value is nearly a square antiprism. However, for Dy2 ion the α angles are 54.48(0)º, 56.07(0)º, 54.52(1)º, and 64.54(10)º, indicating large deviations from the ideal value. This is most likely due to the constraints imposed on Dy2 ion of the Schiff base ligands. The two square antiprisms share two oxygen atoms, O1 and O8a.

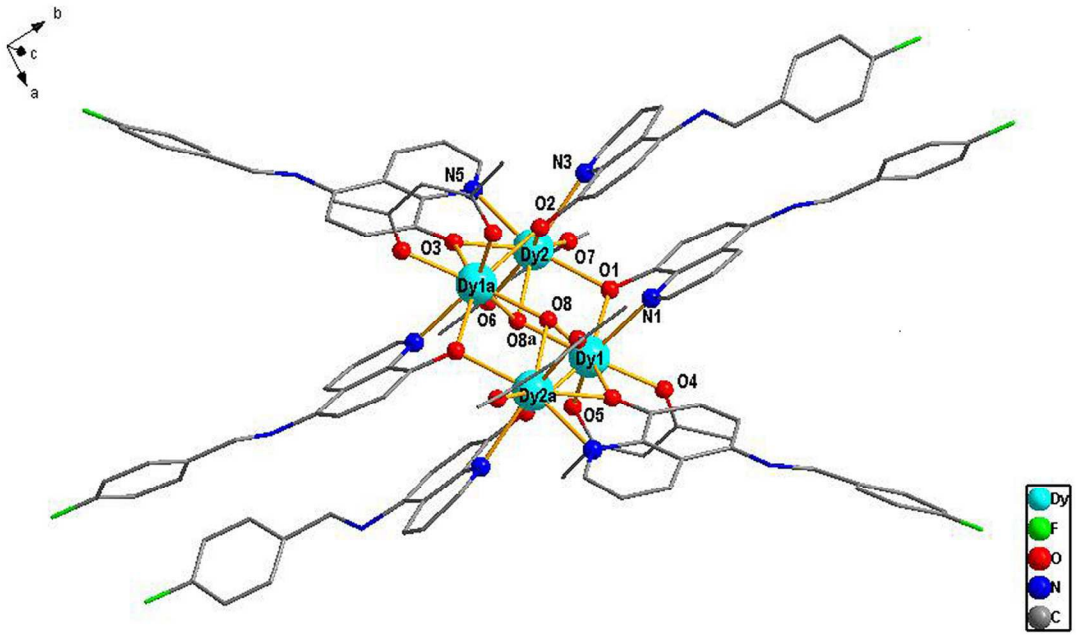

Fig. 1 Molecular structure of **5**, all hydrogen atoms and the overlapping fluorophenyl rings have been omitted for clarity.

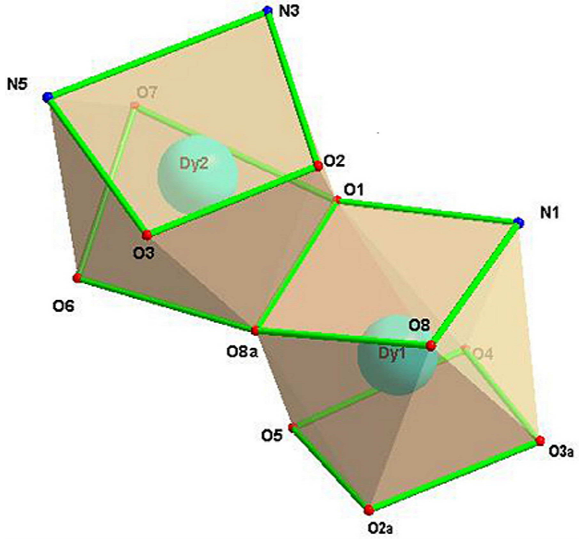

Fig. 2 Coordination polyhedrons for the adjacent Dy(III) ions in complex **5**.

All 8-coordinated Dy(III) ions are linked together by a combination of the two oxygen atoms (O8, O8a) of the μ_3-OH ligands and phenoxo oxygen atoms (O1, O2, O3, O1a, O2a, O3a). There are four bidentate anionic acac$^-$ groups above and below the planar core coordinating to four

Dy(III) ions, respectively. The four Dy(III) ions are precisely coplanar (Fig. 3a), and two triply bridging hydroxide (O8, O8a) atoms lie approximately 0.8942 Å above and below the Dy_4 plane. The μ_3-OH groups form near symmetrical bridges to the metal centers, with Dy2–O8, Dy1–O8, and Dy1a–O8 distances of 2.342(2), 2.340(3), and 2.378(2) Å, respectively, as well as Dy1a–O8–Dy2, Dy1–O8–Dy1a, and Dy1–O8–Dy2 angles of 98.28(12)º, 108.36(13)º, and 112.55(13)º, respectively. Finally, the four Dy(III) ions are located at the corners of a parallelogram. The shortest intramolecular Dy···Dy distance of 3.5659(6) Å is on the edge of the parallelogram (Fig. 3b) between Dy1 and Dy2a as well as Dy1a and Dy2. The Dy–O distances in **5** are in the range of 2.299(3)–2.443(4) Å, the Dy–N bond lengths are in the range of 2.509(5)–2.551(5) Å and the O–Dy–O angles are in the range of 66.49(12)º–147.50(11)º.

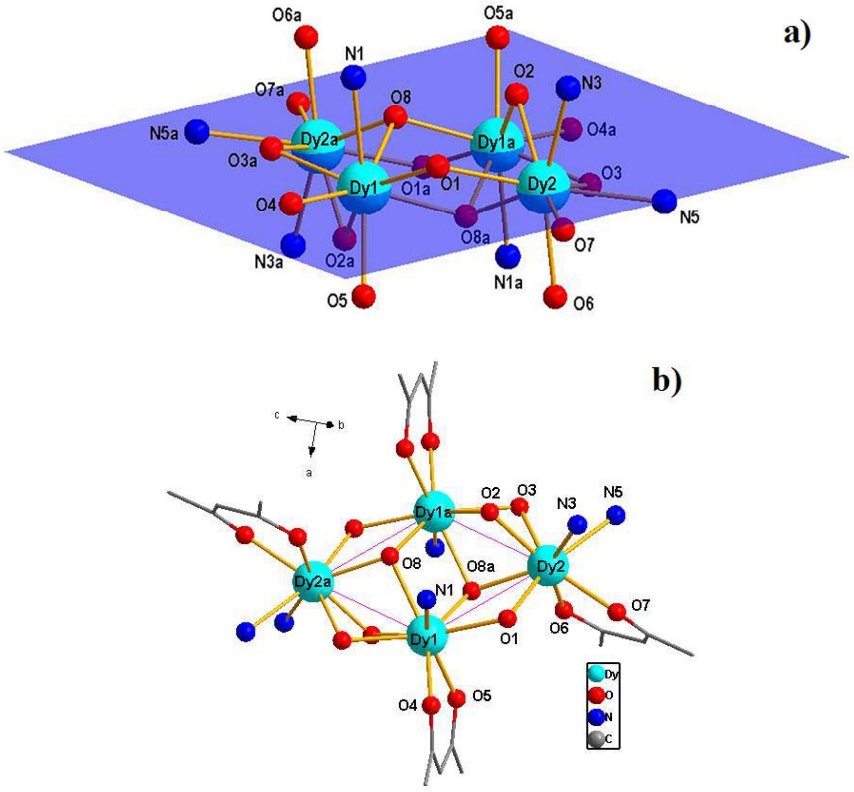

Fig. 3 a) Side view of the planar Dy_4 core; b) parallelogram view of complex **5** with partial HL omitted for clarity.

PXRD and TGA. The experimental Powder X-ray diffraction (PXRD) patterns for the bulk samples of **1**−**7** were obtained to confirm the phase purity (Fig. S2†). The main peaks displayed

in the measured patterns matched well with the simulated patterns generated from single-crystal X-ray diffraction data. Several missing or extra minor peaks could be attributed to the loss of the solvent molecules in the unit cell during the sample preparation, which is unavoidable.

To study the complexes more fully with respect to the thermal stability, the thermal behaviors of **1**–**7** were examined on the crystalline samples under air atmosphere from 30 to 800 °C by thermo-gravimetric analyses (TGA). The crystalline samples were kept for a period of time at ambient conditions resulting in the solvent molecules losing spontaneously, so there are no solvent loss occurs in the 30–100 °C range (Fig. S3†). Integral tendencies of all the TG curves are very similar, which display a main weight loss taking place between 250 and 700 °C, related to the release of organic ligands.

UV-Vis Spectra. The UV-vis absorption spectra of complexes **1**−**7**, the metal precursor $Dy(acac)_3 \cdot 2H_2O$ and HL were measured in methanol solution (10^{-4} mol·L^{-1}) at ambient temperature (Fig. 4). In methanol solution, $Dy(acac)_3 \cdot 2H_2O$ displays a single intense absorption band at ca. 292 nm resulting from intra-ligand (acac) $\pi \rightarrow \pi^*$ transitions. HL consists of three main absorption bands centered at ca. 210, 249, and 368 nm, respectively. In contrast, complexes **1**−**7** display three analogous sets of absorption bands at ca. 209, 262, and 408 nm, respectively. The observed main peaks at ca. 262 nm might be attributed to the intra-ligand transitions of L^- and $acac^-$ ligands. And the distinct absorption bands at 408 nm of complexes **1**−**7** can be ascribed most likely to the extended $n \rightarrow p^*$ transitions in Schiff base ligands bound to the RE(III) ions. In addition, the broad low energy band is distinctly red-shifted compared to that of the free Schiff base ligand, which might be assigned to the coordination effect between the Schiff base ligand and RE(III) cations.

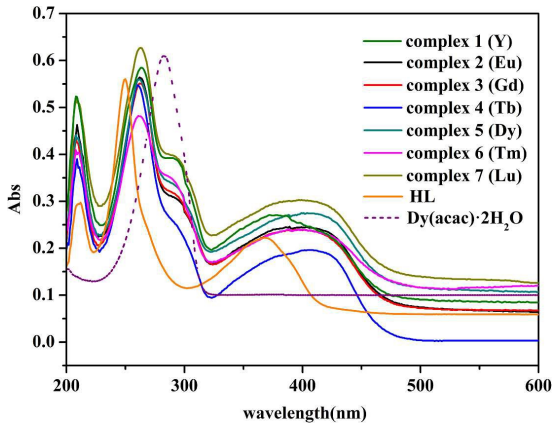

Fig. 4 UV-vis absorption spectra of complexes **1**–**7**, HL and $Dy(acac)_3 \cdot 2H_2O$.

Photophysical properties. The photoluminescence of complexes **1, 2, 4, 5, 7** were recorded in methanol solution (10^{-5} mol·L^{-1}) at ambient temperature. The characteristic peak of Eu(III) ion at 617 nm was observed when complex **2** was excited at 307nm (Fig. 5a). However, the emission spectrum of complex **4** exhibits four major Tb(III) emission peaks at 492, 545, 589 and 621 nm. The first emission band at 492 nm can be assigned to the transitions of $^5D_4 \rightarrow {}^7F_6$, while the other bands at 545, 589, and 621 nm can be attributed to the $^5D_4 \rightarrow {}^7F_5$, $^5D_4 \rightarrow {}^7F_4$, and $^5D_4 \rightarrow {}^7F_3$ transitions, respectively (Fig. 5b). For **5**, the typical luminescence peaks at 482 and 574 nm can be assigned to the transitions of $^4F_{9/2} \rightarrow {}^6H_{15/2}$ and $^4F_{9/2} \rightarrow {}^6H_{13/2}$, respectively (Fig. 5c). The yellow emission intensity of the $^4F_{9/2} \rightarrow {}^6H_{13/2}$ transition is much stronger than that of the blue $^4F_{9/2} \rightarrow {}^6H_{15/2}$ transition, suggesting that the ligand is suitable for the sensitization of yellow luminescence of Dy(III), as are those in other similar complexes.[21] In addition, the emission spectrum of complex **4** in solid state has been obtained (Fig. 5d), while the emission peaks of complexes **2** and **5** in solid state cannot be detected. The different performances between the complexes are related to the energy matching between the excited states of the RE(III) ion and the triplet state of the organic ligands. It is easy to find that the energy transfer from the organic ligands to Tb(III) is more effective than to Eu(III) or Dy(III). For complexes **1** and **7**, due to the full-filled 4f orbital electron configuration of yttrium and lutetium ions, they would not show their typical emission peaks. The main emission bands shown in Fig. 5e can be attributed to $\pi \rightarrow \pi^*$ transitions of the ligand. When complexes **1** and **7** were excited at 262 nm where the ligand absorption mainly takes place, the emission spectra of them exhibit several major emission peaks consistent with the ligand in methanol solution. From the emission spectra, the luminescence

intensities of the two complexes are not higher than that of the free ligand, indicating that yttrium ion and lutetium ion cannot induce the luminescence enhancement for the ligand.

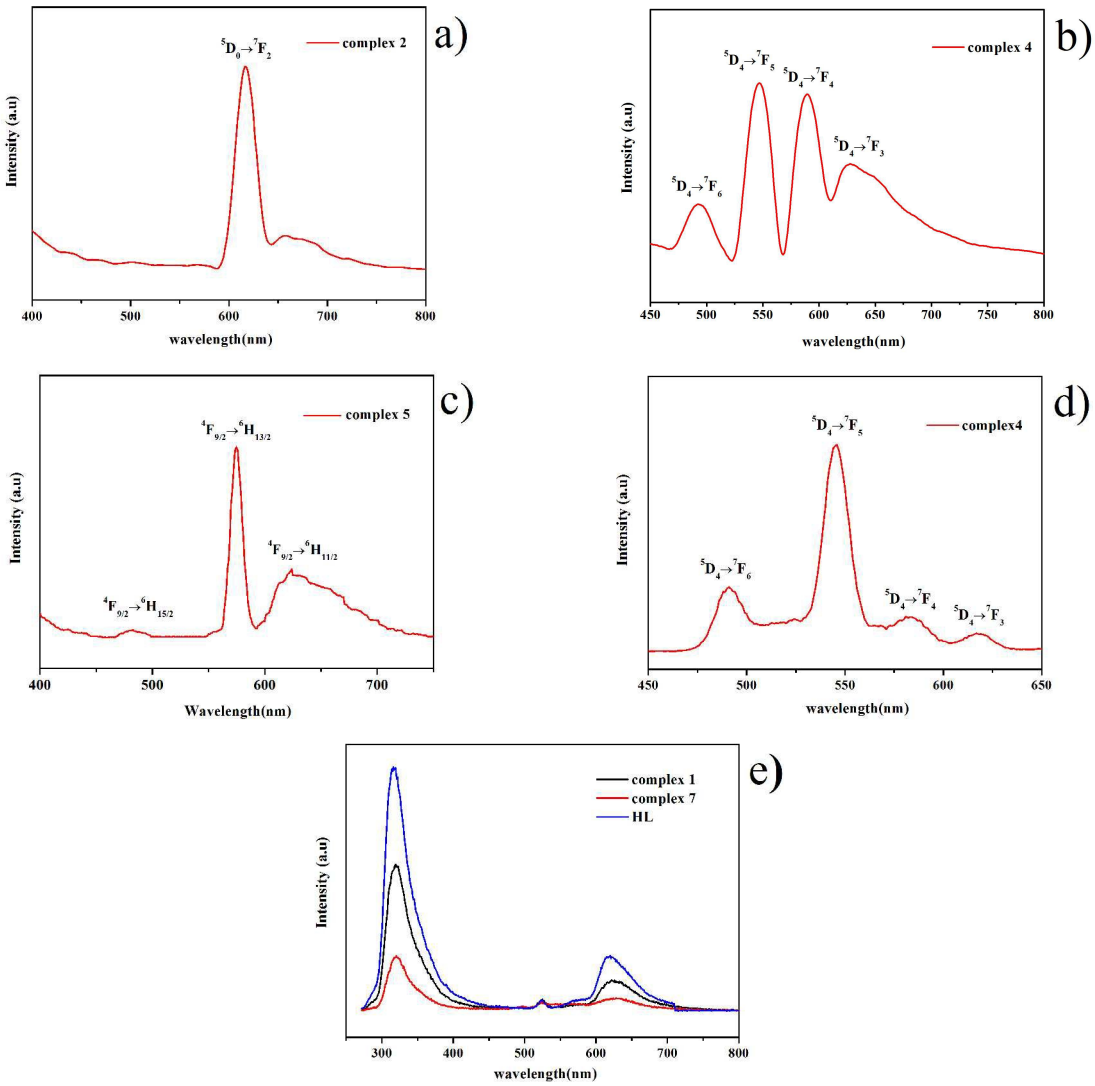

Fig. 5 a) The luminescence spectrum of complex **2** in methanol solution; b) the luminescence spectrum of complex **4** in methanol solution; c) the luminescence spectrum of complex **5** in methanol solution; d) the luminescence spectrum of complex **4** in solid state; e) the luminescence spectra of complexes **1**, **7** and HL in methanol solution.

Magnetic properties. The crystalline samples for all magnetic measurements were desolvated to avoid the influence of the interstitial solvent molecules on the magnetic measurements.

The temperature dependence of the magnetic susceptibilities studies for complexes **3**, **4**, **5**, **6**

were carried out in an applied dc magnetic field of 1000 Oe in the temperature range of 2−300 K (Fig. 6). For **3**, the observed room-temperature $\chi_M T$ value is 32.92 cm^3 K mol^{-1}, slightly higher than the theoretical value of 31.52 cm^3 K mol^{-1} for four uncoupled Gd(III) ions ($^8S_{7/2}$, $g = 2$).[22] As shown in Fig. 6, during the cooling process, the $\chi_M T$ remains almost invariable in the temperature range of 300−60 K, and then decreases sharply, reaching a minimum value of 15.13 cm^3 K mol^{-1} at 2 K. The downward slope in $\chi_M T$ tending toward zero at base temperatures can only be attributed, in the absence of any zero-field splitting or close contacts with other molecules, to a weak intramolecular antiferromagnetic exchange between the Gd(III) centers. Negative value of θ further supports the occurrence of the antiferromagnetic coupling between the Gd(III) ions (Fig. S4†). For complex **4**, the $\chi_M T$ value at room temperature is 46.47 cm^3 K mol^{-1}, close to the expected value of 47.28 cm^3 K $mol^{-1}$for four uncoupled Tb(III) ions (**$^7F_6$, $g = 3/2$**). This value is almost a constant from 300 to 100 K, and then gradually reduces to 34.91 cm^3 K mol^{-1} at 2 K upon further cooling. This phenomenon may arise from the ferromagnetic interaction compensating the decrease of $\chi_M T$ value originated from the depopulation of Stark sublevels.[23] For **5** and **6**, the $\chi_M T$ values at room temperature are 59.83 and 29.03 cm^3 K mol^{-1}, respectively. The value of 29.03 cm^3 K $mol^{-1}$is close to the expected value of 28.60 cm^3 K $mol^{-1}$for four uncoupled Tm(III) ions ($^3H_6$, $g = 7/6$), while the value of 59.83 cm^3 K mol^{-1} is higher than the expected value of 56.68 cm^3 K mol^{-1} for four uncoupled Dy(III) ions ($^6H_{15/2}$, $g = 4/3$). As the temperature is decreased, the $\chi_M T$ values of **5** and **6** decrease gradually and reach a minimum of 30.64 and 15.30 cm^3 K mol^{-1} at 2 K, respectively. This can be probably attributed to a combination of the antiferromagnetic interaction between the Ln(III) ions and/or the thermal depopulation of excited Stark sublevels.[10j, 23]

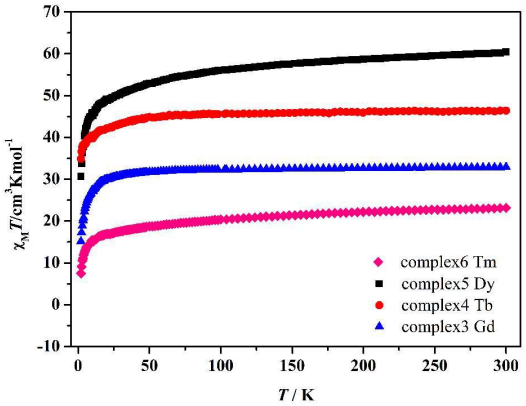

Fig. 6 Temperature dependence of the $\chi_M T$ product for complexes **3**, **4**, **5**, **6** at 2−300K with a dc

applied field of 1000 Oe.

To investigate the dynamics of the magnetization, the temperature dependence of ac magnetic susceptibilities for complexes **4** and **5** were characterized at the indicated frequencies (111−2311 Hz) under an oscillating ac field of 3 Oe. As shown in Fig. 7, the out-of-phase component χ'' of complex **5** deviates from zero and both χ' and χ'' become frequency-dependent below 20 K. A peculiar feature of these curves for complex **5** is that several peaks occur. Among them, the peaks around 2K are not complete. Two distinct peaks are frequency-dependent with maxima for χ'' at 7.4 and 15.4 K for 2311 Hz, revealing the occurrence of two remarkable relaxation processes. This behavior has been described in recent reports,[11a-f] and can be attributed to the presence of two metal sites in the crystal lattice. For complex **4**, the imaginary component χ_M'' does not show any positive value even at 2.0 K under zero dc field. (Fig. S5†) Thus, we do not think complex **4** expresses SMM behavior even at low temperature.

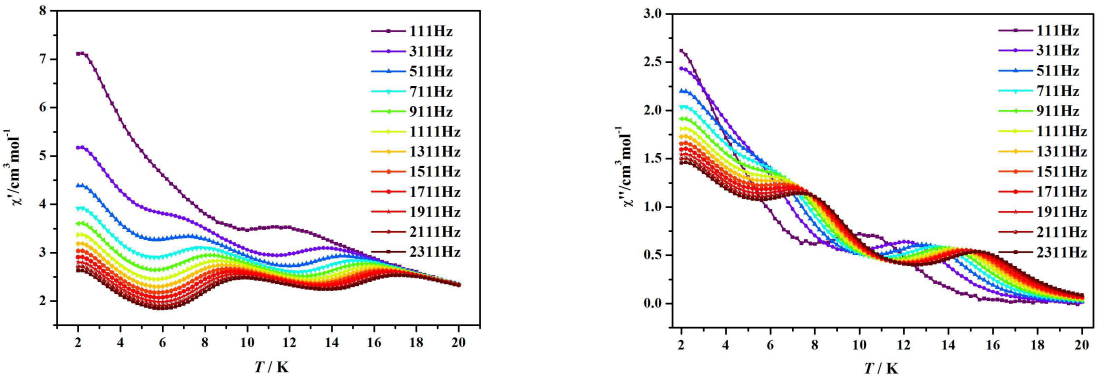

Fig. 7 Temperature dependence of the ac susceptibility for complex **5** as a function of the temperature below 20 K under an oscillating ac field of 3 Oe.

To better understand the nature of the two types of dynamics, a further investigation was conducted on complex **5** by a thorough in-of-phase (χ') and out-of-phase (χ'') versus frequency (ν) measurement at temperatures ranging from 2 to 16 K under zero dc field (Fig. 8). The relaxation time of **5** were extracted from the two ridges of the frequency-dependent data by fitting the Lorentzian peak function to the χ'' versus frequency curves, illustrating two relaxation processes corresponding to the high-frequency peaks (fast relaxation phase, FR) and the low-frequency peaks (slow relaxation phase, SR). Two sets of relaxation parameters in the format of $\ln(\tau)$ versus $1/T$ plots were analyzed using the Arrhénius law, $\tau = \tau_0 \exp(U_{eff}/k_B T)$, giving two effective energy

barriers, with U_{eff} = 48 K (τ_0 = 2.2×10^{-7} s) and U_{eff} = 121 K (τ_0 = 2.8 × 10^{-8} s) for the SR and FR, respectively (Fig. 9). Both τ_0 values are in the expected range of 10^{-6}–10^{-11} s for the SMMs reported previously.[7] It is worth mentioning that the latter effective barrier of 121 K is a relatively high value among the multi-relaxations Dy_4 SMMs under zero dc field.[11c-e]

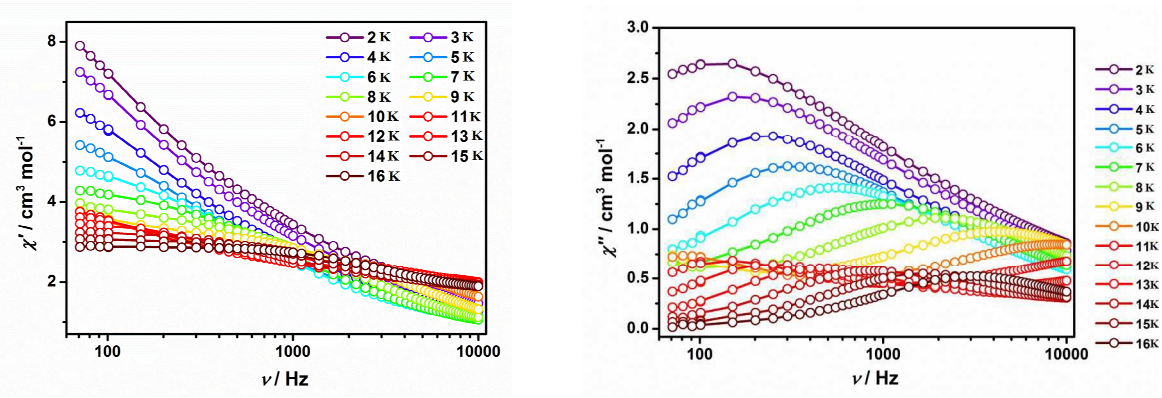

Fig. 8 Frequency dependence of the ac susceptibility for complex **5** as a function of the ac frequency between 1 and 10000 Hz under H_{ac} = 3 Oe.

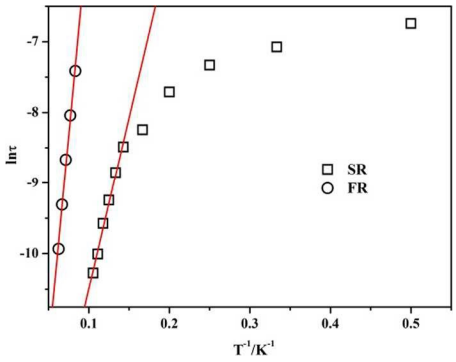

Fig. 9 ln τ vs. T^{-1} plot for complex **5** under H_{ac} = 3 Oe. The solid lines are fitted with the Arrhenius law for SR and FR, respectively.

Cole–Cole diagrams (Fig. 10) in the form of χ'' versus χ' have also been obtained. These data for each relaxation process have been fitted by the generalized Debye model, giving the distribution coefficient values of α_1(0.29–0.55) and α_2(0.069–0.21) for the SR and FR, respectively.(Table S2†) Both the α_1 values and α_2 values are big, implying that both thermally activated relaxation processes have a wide distribution of relaxation time, which is related to the presence of two crystallographically independent Dy(III) sites.

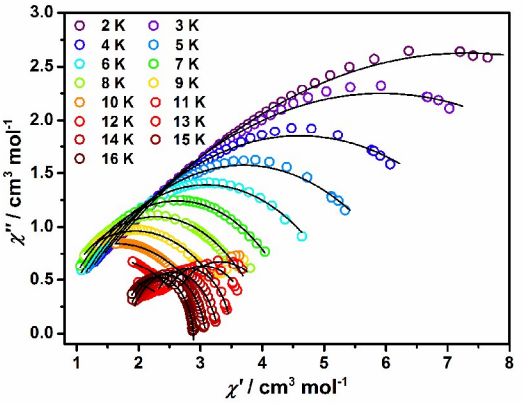

Fig. 10 Cole-Cole plots at 2–16 K for complex **5** (H_{dc} = 0 Oe and H_{ac} = 3 Oe), the solid lines represent the best fitting with the generalized Debye model.

The feature of complex **3** is promising for a large low-temperature magnetocaloric effect (MCE) because the possible magnetic entropy change on magnetization is enhanced by the multiple low-lying states that are thermally accessible in zero-field (large entropy) while the magnetization can still be saturated (zero entropy) in applied field.[24] The isothermal magnetization from 2 K to 10 K were measured (Fig. 11a). The magnetization increases steadily with the applied dc field and reaches the saturation value of 28.04 $N\beta$ at 2 K and 8 T, which is close to the theoretical saturation value for four Gd(III) ions with g = 2. The isothermal entropy change can be calculated by applying the Maxwell equation (Fig. 11b):

$$-\Delta S_m(T) = \int_0^H [\partial M(T,H)/\partial T]_H dH$$

In general, the $-\Delta S_m$ values increase gradually as the temperature is reduced, but rise progressively with increasing applied fields, reaching a maximum of 20.8 J kg^{-1} K^{-1} at T = 3 K and ΔH = 8 T, which is lower than the theoretical limiting value of 26.1 J kg^{-1} K^{-1} calculated from nRln $(2S + 1)/M$w, with S = 7/2, and Mw = 2651 g mol^{-1}. This difference between experimental and theoretical values may be attributed to the antiferromagnetic interactions.[25]

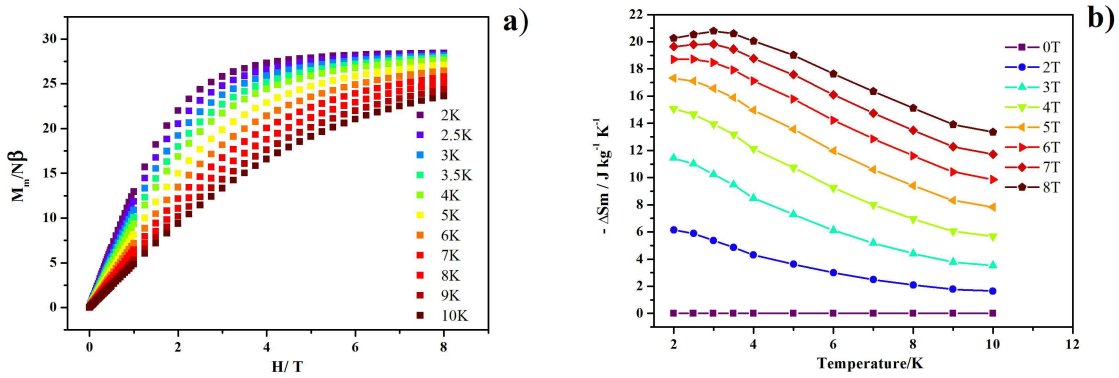

Fig. 11 a) Magnetization versus the dc field in the temperature range of 2–10 K for complex **3**; b) temperature-dependencies of $-\Delta S_m$ for selected ΔH obtained from magnetization, and the data with field variation between 0−2 T are omitted for clarity.

CONCLUSION

In summary, we have successfully constructed seven new functional rare earth complexes with a typical butterfly or rhombus topology. Complex **5** exhibits multiple zero-field slow magnetic relaxations behavior which could enlarge the available database and thus improve the current knowledge of the structure-property relationship in lanthanide containing SMMs. The magnetocaloric effect was detected for complex **3**, but, as we have seen, magnetic entropy change (20.8 J kg^{-1} K^{-1}) is not large enough for a better magnetic cooling material. Better Gd(III)-based magnetic coolers should be always commensurate with a high metal/ligand ratio. The fact that the best performance found so far in the field has been in Gd(III) polymers incorporating small ligands[24g-h] further exemplifies this point. The employment of 8-hydroxyquinoline-based Schiff base as an important moiety of the ligand would provide a route toward the design of novel fluorescent and magnetic materials.

AUTHOR INFORMATION

Corresponding Author

*E-mail: cuijianzhong@tju.edu.cn.

Notes

The authors declare no competing financial interest.

ACKNOWLEDGEMENT

This work was supported financially by the National Natural Science Foundation of China (Nos. 21473121, 21271137, 21571138).

REFERENCES

1 (a) J. Long, J. Rouquette, J. M. Thibaud, R. A. Ferreira, L. D. Carlos, B. Donnadieu, V. Vieru, L. F. Chibotaru, L. Konczewicz, J. Haines, Y. Guari, J. Larionova, *Angew. Chem.*, *Int. Ed.*, 2015, **54**, 2236–2240; (b) P. H. Guo, Y. Meng, Y. C. Chen, Q. W. Li, B. Y. Wang, J. D. Leng, D. H. Bao, J. H. Jia, M. L. Tong, *J. Mater. Chem. C*, 2014, **2**, 8858–8864; (c) P. H. Guo, J. L. Liu, J. H. Jia, J. Wang, F. S. Guo, Y. C. Chen, W. Q. Lin, J. D. Leng, D. H. Bao, X. D. Zhang, J. H. Luo, M. L. Tong, *Chem. Eur. J.*, 2013, 19, 8769–8773; (d) H. S. Qian, Y. Hu, Z. Q. Li, X. Y. Yang, L. C. Li, X. T. Zhang, R. Xu, *J. Phys. Chem. C*, 2010, **114**, 17455–17459; (e) L. Tong, J. Shi, D. Liu, Q. Li, X. Ren, H. Yang, *J. Phys. Chem. C*, 2012, **116**, 7153–7157.

2 (a) C. Dossantos, A. Harte, S. Quinn, T. Gunnlaugsson, *Coord. Chem. Rev.*, 2008, **252**, 2512–2527; (b) L. E. Kreno, K. Leong, O. K. Farha, M. Allendorf, R. P. Van Duyne, J. T. Hupp, *Chem. Rev.*, 2012, **112**, 1105–1125; (c) X. D. Wang, O. S. Wolfbeis, R. J. Meier, *Chem. Soc. Rev.*, 2013, **42**, 7834–7869; (d) S. Silvi, A. Credi, *Chem. Soc. Rev.*, 2015, **44**, 4275–4289.

3 W. Wernsdorfer, N. Aliaga-Alcalde, D. N. Hendrickson, G. Christou, *Nature*, 2003, **416**, 406–410.

4 (a) W. Wernsdorfer, R. Sessoli, *Science*, 1999, **284**, 133–135; (b) L. B. Wernsdorfer, *Nat. Mater.*, 2008, **7**, 179–186.

5 (a) M. N. Leuenberger, D. Loss, *Nature*, 2001, **410**, 789–793; (b) S. Hill; R. S. Edwards, N. Aliaga-Alcalde, G. Christou, *Science*, 2003, **302**, 1015–1018.

6 (a) F. Habib, G. Brunet, V. Vieru, I. Korobkov, L. F. Chibotaru, M. Murugesu, *J. Am. Chem. Soc.*, 2013, **135**, 13242–13245; (b) Y. N. Guo, G. F. Xu, W. Wernsdorfer, L. Ungur, Y. Guo, J. Tang, H. J. Zhang, L. F. Chibotaru, A. K. Powell, *J. Am. Chem. Soc.*, 2011, **133**, 11948–11951; (c) R. J. Blagg, L. Ungur, F. Tuna, J. Speak, P. Comar, D. Collison, W. Wernsdorfer, E. J. L. McInnes, L. F. Chibotaru, R. E. P. Winpenny, *Nat. Chem.*, 2013, **5**, 673–678; (d) J. Long, R. Vallat, R. A. S. Ferreira, L. D. Carlos, F. A. A. Paz, Y. Guari, J. Larionova, *Chem. Commun.*, 2012, **48**, 9974–9976; (e) S. D. Jiang, B. W. Wang, H. L. Sun, Z. M. Wang; S. Gao, *J. Am. Chem. Soc.*, 2011, **133**, 4730–4733; (f) R. J. Blagg, C. A. Muryn, E. J. L. McInnes, F. Tuna, R.

E. P. Winpenny, *Angew. Chem., Int. Ed.*, 2011, **50**, 6530–6533; (g) J. W. Sharples, D. Collison, *Polyhedron*, 2013, **54**, 91–103; (h) J. W. Sharples, Y. Z. Zheng, F. Tuna, E. J. L. McInnes, D. Collison, *Chem. Commun.*, 2011, **47**, 7650–7652; (i) Y. C. Chen, L. Qin, Z. S. Meng, D. F. Yang, C. Wu, Z. Fu, Y. Z. Zheng, J. L. Liu, R. Tarasenko, M. Orendáč, J. Prokleška, V. Sechovský, M. L. Tong, *J. Mater. Chem.*, 2014, **2**, 9851–9858.

7 (a) R. Sessoli, D. Gatteschi, A. Caneschi, M. A. Novak, *Nature*, 1993, **365**, 141–143; (b) F. Mori, T. Nyui, T. Ishida, T. Nogami, K. Y. Choi, H. Nojiri, *J. Am. Chem. Soc.*, 2006, **128**, 1440–1441; (c) P. H. Lin, T. J. Burchell, R. Clérac, M. Murugesu, *Angew. Chem., Int. Ed.*, 2008, **47**, 8848–8851; (d) A. R. Tomsa, J. Martinez-Lillo, Y. Li, L. M. Chamoreau, K. Boubekeur, F. Farias, M. A. Novak, E. Cremades, E. Ruiz, A. Proust, M. Verdaguer, P. Gouzerh, *Chem. Commun.*, 2010, **46**, 5106–5108; (e) G. Abbas, Y. H. Lan, G. E. Kostakis, W. Wernsdorfer, C. E. Anson, A. K. Powell, *Inorg. Chem.*, 2010, **49**, 8067–8072; (f) J. D. Rinehart, M. Fang, W. J. Evans, J. R. Long, *J. Am. Chem. Soc.*, 2011, **133**, 14236–14239; (g) M. Andruh, *Chem. Commun.*, 2011, **47**, 3025–3042; (h) V. Mereacre, Y. Lan, R. Clerac, A. M. Ako, W. Wernsdorfer, G. Buth, C. E. Anson, A. K. Powell, *Inorg. Chem.*, 2011, **50**, 12001–12009; (i) J. L. Liu, Y. C. Chen, Y. Z. Zheng, W. Q. Lin, L. Ungur, W. Wernsdorfer, L. F. Chibotaru, M. L. Tong, *Chem. Sci.*, 2013, **4**, 3310–3316; (j) J. Martinez-Lillo, N. Dolan, E. K. Brechin, *Dalton Trans.*, 2014, **43**, 4408–4414; (k) J. W. Sharples, D. Collison, *Coord. Chem. Rev.*, 2014, **260**, 1–20; (l) F. Luan, T. Liu, P. Yan, X. Zou, Y. Li, G. Li, *Inorg. Chem.*, 2015, **54**, 3485–3490; (m) P. Zhang, L. Zhang, J. Tang, *Dalton Trans.*, 2015, **44**, 3923–3929.

8 (a) J. J. Sokol, A. G. Hee, J. R. Long, *J. Am. Chem. Soc.*, 2002, **124**, 7656–7657; (b) R. Sessoli, A. K. Powell, *Coord. Chem. Rev.*, 2009, **253**, 2328–2341; (c) O. G. Aromi, E. K. Brechin, *Struct. Bonding (Berlin, Ger.)*, 2006, **122**, 1–67; (d) M. Ren, S. S. Bao, N. Hoshino, T. Akutagawa, B. Wang, Y. C. Ding, S. Wei, L. M. Zheng, *Chem. Eur. J.*, 2013, **19**, 9619–9628; (e) C. Y. Chow, H. Bolvin, V. E. Campbell, R. Guillot, J. W. Kampf, W. Wernsdorfer, F. Gendron, J. Autschbach, V. L. Pecoraro, T. Mallah, *Chem. Sci.*, 2015, **6**, 4148–4159; (f) V. E. Campbell, H. Bolvin, E. Riviere, R. Guillot, W. Wernsdorfer, T. Mallah, *Inorg. Chem.*, 2014, **53**, 2598–2605.

9 (a) D. N. Woodruff, R. E. Winpenny, R. A. Layfield, *Chem. Rev.*, 2013, **113**, 5110–5148; (b) F. Habib, M. Murugesu, *Chem. Soc. Rev.*, 2013, **42**, 3278–3288.

10 (a) S. Y. Lin, J. K. Tang, *Polyhedron*, 2014, **83**, 185–196; (b) J. Liu, Y. C. Chen, Z. X. Jiang, J. L. Liu, J. H. Jia, L. F. Wang, Q. W. Li, M. L. Tong, *Dalton Trans.*, 2015, **44**, 8150–8155; (c) H. H. Zou, R. Wang, Z. L. Chen, D. C. Liu, F. P. Liang, *Dalton Trans*., 2014, **43**, 2581–2587; (d) D. N. Woodruff, F. Tuna, M. Bodensteiner, R. E. P. Winpenny, R. A. Layfield, *Organometallics*, 2013, **32**, 1224–1229; (e) P. Zhang, L. Zhang, C. Wang, S. Xue, S. Y. Lin, J. Tang, *J. Am. Chem. Soc.*, 2014, **136**, 4484–4487; (f) M. Feng, F. Pointillart, B. Lefeuvre, V. Dorcet, S. Golhen, O. Cador, L. Ouahab, *Inorg. Chem.,* 2015, **54**, 4021–4028; (g) F. Yang, Q. Zhou, G. Zeng, G. Li, L. Gao, Z. Shi, S. Feng, *Dalton Trans.*, 2014, **43**, 1238–1245; (h) J. Tang, I. Hewitt, N. T. Madhu, G. Chastanet, W. Wernsdorfer, C. E. Anson, C. Benelli, R. Sessoli, A. K. Powell, *Angew. Chem., Int. Ed.,* 2006, **45**, 1729–1733; (i) M. T. Gamer, Y. H. Lan, P. W. Roesky, A. K. Powell, R. Cle´rac, *Inorg. Chem.,* 2008, **47**, 6581–6583; (j) J. B. Peng, X. J. Kong, Y. P. Ren, L. S. Long, R. B. Huang, L. S. Zheng, *Inorg. Chem.*, 2012, **51**, 2186–2190.

11 (a) P. H. Lin, T. J. Burchell, L. Ungur, L. F. Chibotaru, W. Wernsdorfer, M. Murugesu, *Angew. Chem., Int. Ed.*, 2009, **48**, 9489–9492; (b) Y. N. Guo, G. F. Xu, P. Gamez, L. Zhao, S. Y. Lin, R. P. Deng, J. K. Tang, H. J. Zhang, *J. Am. Chem .Soc.*, 2010, **132**, 8538–8539; (c) P. H. Lin, W. B. Sun, M. F. Yu, G. M. Li, P. F. Yan, M. Murugesu, *Chem. Commun.*, 2011, **47**, 10993–10995; (d) C. M. Liu, D. Q. Zhang, D. B. Zhu, *Dalton Trans*., 2013, **42**, 14813–14818; (e) S. Das, A. Dey, S. Biswas, E. Colacio, V. Chandrasekhar, *Inorg. Chem.*, 2014, **53**, 3417–3426; (f) P. H. Guo, J. Liu, Z. H. Wu, H. Yan, Y. C. Chen, J. H. Jia, M. L. Tong, *Inorg. Chem.*, 2015, **54**, 8087–8092; (g) P. F. Yan, P. H. Lin, F. Habib, T. Aharen, M. Murugesu, Z. P. Deng, G. M. Li, W. B. Sun, *Inorg. Chem.*, 2011, **50**, 7059–7065; (h) P. H. Guo, J. L. Liu, Z. M. Zhang, L. Ungur, L. F. Chibotaru, J. D. Leng, F. S. Guo, M. L. Tong, *Inorg. Chem.*, 2012, **51**, 1233–1235; (i) V. Chandrasekhar, S. Hossain, S. Das, S. Biswas, J. P. Sutter, *Inorg. Chem.*, 2013, **52**, 6346–6353; (j) M. Yadav, V. Mereacre, S. Lebedkin, M. M. Kappes, A. K. Powell, P. W. Roesky, *Inorg. Chem.*, 2015, **54**, 773–781.

12 (a) S. D. Jiang, B. W. Wang, G. Su, Z. M. Wang, S. Gao, *Angew. Chem., Int. Ed.*, 2010, **49**, 7448–7451; (b) H. Q. Tian, L. Zhao, Y. N. Guo, Y. Guo, J. K. Tang, Z. L. Liu, *Chem. Commun.*, 2012, **48**, 708–710; (c) W. B. Sun, B. L. Han, P. H. Lin, H. F. Li, P. Chen, Y. M. Tian, M. Murugesu, P. F. Yan, *Dalton Trans.*, 2013, **42**, 13397–13403; (d) F. Luan, P. Yan, J. Zhu, T. Liu, X. Zou, G. Li, *Dalton Trans.*, 2015, **44**, 4046–4053.

13 (a) M. Makowska-Janusik, E. Gondek, I. V. Kityk, J. Wisla, J. Sanetra, A. Danel, *Chem. Phys.*, 2004, **306**, 265–271; (b) E. Koscien, J. Sanetra, E. Gondek, B. Jarosz, I. Kityk, J. Ebothe, A. V. Kityk, *Opt. Commun.*, 2004, **242**, 401–409; (c) N. M. Shavaleev, R. Scopelliti, F. Gumy, J. C. G. Bunzli, *Inorg. Chem.*, 2009, **48**, 2908–2918.

14 (a) G. F. de Sa, O. L. Malta, C. D. Donega, A. M. Simas, R. L. Longo, P. A. Santa-Cruz, E. F. da Silva, *Coord. Chem. Rev.*, 2000, **196**, 165–195; (b) K. Binnemans, C. Gorller-Walrand, *Chem. Rev.*, 2002, **102**, 2303–2345.

15 K. Bernot, J. Luzon, L. Bogani, M. Etienne, C. Sangregorio, M. Shanmugam, A. Caneschi, R. Sessoli, D. Gatteschi, *J. Am. Chem. Soc.*, 2009, **131**, 5573–5579.

16 (a) L. R. Melby, E. Abramson, J. C. Caris, *J. Am. Chem. Soc.*, 1964, **86**, 5117–5125; (b) S. Katagi ri, Y. Tsukahara, Y. Hasegawa, Y. Wada, *Bull. Chem. Soc. Jpn.*, 2007, **80**, 1492–1503.

17 (a) *Theory and Applications of Molecular Paramagnetism*; Boudreaux, E. A., Mulay, L. N., Eds.; Wiley-Interscience: New York, 1976; (b) G. A. Bain, J. F. Berry, *J. Chem. Educ*., 2008, **85**, 532–536.

18 A. Lilienkampf, J. L. Mao, B. J. Wan, Y. H. Wang, S. G. Franzblau, A. P. Kozikowski, *J. Med. Chem.*, 2009, **52**, 2109–2118.

19 G. M. Sheldrick, *Acta Crystallogr.*, *Sect. A: Found. Crystallogr.*, 2008, **64**, 112–122.

20 (a) H. S. Ke, P. Gamez, L. Zhao, G. F. Xu, S. F. Xue, J. K. Tang, *Inorg. Chem.*, 2010, **49**, 7549–7557; (b) S. Adam, A. Ellern, K. Seppelt, *Chem. Eur. J.*, 1996, **2**, 398–402.

21 (a) J. Ruiz, A. J. Mota, A. RodriguezDieguez, S. Titos, J. M. Herrera, E. Ruiz, E. Cremades, J. P. Costes, E. Colacio, *Chem. Commun.*, 2012, **48**, 7916−7918; (b) Y. L. Wang, Y. Ma, X. Yang, J. Tang, P. Cheng, Q. L. Wang, L. C. Li, D. Z. Liao , *Inorg. Chem.*, 2013, **52**, 7380−7386.

22 (a) D. Aguilam, L. A. Barrios, V. Velasco, L. Arnedo, N. Aliaga- Alcalde, M. Menelaou, S. J. Teat, O. Roubeau, F. Luis, G. Aromí, *Chem.−Eur. J.*, 2013, **19**, 5881–5891; (b) L. Cañadillas-Delgado, J. Pasan, O. Fabelo, M. Hernandez-Molina, F. Lloret, M. Julve, C. Ruiz-Perez, *Inorg. Chem.*, 2006, **45**, 10585–10594; (c) N. Xu, W. Shi, D. Z. Liao, S. P. Yan, P. Cheng, *Inorg. Chem.*, 2008, **47**, 8748–8756; (d) S. T. Hatscher, W. Urland, *Angew. Chem., Int. Ed.*, 2003, **42**, 2862–2864; (e) J. P. Costes, J. M. Clemente-Juan, F. Dahan, F. Nicodeme, M. Verelst, *Angew. Chem., Int. Ed.*, 2002, **41**, 323–325; (f) R. Baggio, R. Calvo, M. T.

Garland, O. Peña, M. Perec, A. Rizzi, *Inorg. Chem.*, 2005, **44**, 8979–8987; (g) J. Goura, J. P. Walsh, F. Tuna, V. Chandrasekhar, *Inorg. Chem.*, 2014, **53**, 3385-3391.

23 (a) Y. L. Hou, G. Xiong, B. Shen, B. Zhao, Z. Chen, J. Z. Cui, *Dalton Trans.*, 2013, **42**, 3587–3596; (b) J. D. Rinehart, J. R. Long, *Chem. Sci.*, 2011, **2**, 2078–2085; (c) S. K. Langley, B. Moubaraki, C. M. Forsyth, I. A. Gass, K. S. Murray, *Dalton Trans*., 2010, **39**, 1705–1708.

24 (a) M. Evangelisti, E. K. Brechin, *Dalton Trans.*, 2010, **39**, 4672–4676; (b) R. J. Blagg, F. Tuna, E. J. L. McInnes, R. E. P. Winpenny, *Chem. Commun.*, 2011, **47**, 10587–10589; (c) Y. Z. Zheng, M. Evangelisti, R. E. P. Winpenny, *Chem. Sci.*, 2011, **2**, 99–102; (d) J. W. Sharples, D. Collison, E. J. L. McInnes, J. Schnack, E. Palacios and M. Evangelisti, *Nat. Commun.*, 2014, 5; (e) F. S. Guo, J. D. Leng, J. L. Liu, Z. S. Meng and M. L. Tong, *Inorg. Chem.*, 2012, 51, 405–413; (f) J. W. Sharples and D. Collison, in Lanthanides and Actinides in Molecular Magnetism, Wiley-VCH Verlag GmbH & Co. KGaA, 2015, pp. 293-314; (g) J. W. Sharples, D. Collison, *Polyhedron*, 2013, **54**, 91–103; (h) M. Evangelisti, O. Roubeau, E. Palacios, A. Camón, T. N. Hooper, E. K. Brechin, J. J. Alonso, *Angew. Chem., Int. Ed.*, 2011, **50**, 6606–6609.

25 (a) J. B. Peng, Q. C. Zhang, X. J. Kong, Y. P. Ren, L. S. Long, R. B. Huang, L. S. Zheng, Z. Zheng, Angew. Chem., 2011, 50, 10649-10652; (b) Y. Yang, Q. C. Zhang, Y. Y. Pan, L. S. Long, L. S. Zheng, Chem. Commun., 2015, 51, 7317-7320.

Table of Contents

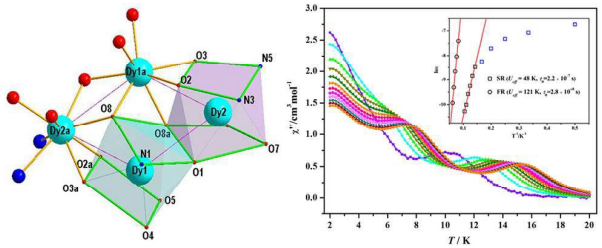

Multi-relaxations single-molecular magnet (SMM) of {Dy_4} complex exhibits two distinct relaxation processes, with the high energy barrier of 121 K.